Flexible Mid-IR fiber bundle for thermal imaging of inaccessible areas

ANDREA VENTURA,[1,*] FEDIA BEN SLIMEN,[1] JORIS LOUSTEAU,[2] NICHOLAS WHITE,[1] ALI MASOUDI,[1] PETR JANICEK,[3,4] AND FRANCESCO POLETTI[1]

[1]*Optoelectronics Research Centre, University of Southampton, Southampton, SO17 1BJ, UK*
[2]*Department of Chemistry and Materials Engineering (CMIC), Politecnico di Milano, Via Mancinelli, 7, 20131 Milano, Italy*
[3]*Institute of Applied Physics and Mathematics, Faculty of Chemical Technology, University of Pardubice, Pardubice, 53210, Czech Republic*
[4]*Center of Materials and Nanotechnologies, Faculty of Chemical Technology, University of Pardubice, Pardubice, 53210, Czech Republic*
*av1d16@soton.ac.uk

Abstract: We present a flexible coherent Mid-Infrared (Mid-IR) fiber bundle for thermal imaging made of 1200 $Ge_{30}As_{13}Se_{32}Te_{25}$ glass cores embedded in a Fluorinated Ethylene Propylene (FEP) polymer cladding. The high index contrast between the chalcogenide glass and the polymer cladding helps minimizing inter-pixel cross-talk, while the low Young's modulus of the polymer cladding gives the bundle good flexibility despite its millimeter scale outer diameter. The delivery of high contrast and high spatial resolution thermal images of a human hand through a 62.5 cm long bundle indicates its excellent imaging potential.

1. Introduction

Today, fields such as military, medical, industrial processing and security rely heavily on the use of thermal imaging techniques, which have benefitted from the continuous development and improvement of optical components such as lenses, filters and detectors that operate in the Mid-Infrared (Mid-IR) wavelength region [1–3]. Thermal imaging captures electromagnetic radiation in the Mid-IR spectral range (3-30 µm), where 'warm' objects emit electromagnetic radiation. Whilst plenty of suitable Mid-IR cameras are available on the market for thermal imaging of accessible objects, no commercial solution currently exists to investigate the thermal characteristics of hard to reach areas, such as the internal structure of a jet engine or the heat shielding plates of a nuclear reactor. Currently, the only instruments available for inspecting such inaccessible locations operate in the visible spectral range and generate non-thermal images. Such instruments rely on flexible and coherent fiber bundles made by stacking together an array of optical fibers, each of which representing a pixel. These fiber bundles were developed in the 1950s to assist medical endoscopy [4] and are now commercially available from multiple suppliers. Thanks to a direct pixel matching between the bundle ends in coherent fiber bundles, images on the input surface can be recreated on the output surface. These are very practical and useful instruments due to the absence of moving optics, high spatial resolution and flexibility.

Fabrication of a practical fiber bundle for the Mid-IR is considerably more challenging for numerous reasons. First, the material choice – often Mid-IR transmitting glasses – are more difficult to draw, more prone to crystallization and with a shorter lifetime than the silica/silicate glasses typically used for the visible spectral range. Then the dimensions of each individual pixels needs to be much larger in order to scale with the wavelength, which makes the fabrication of flexible bundles more challenging. Despite this, several fiber bundles transparent in the Mid-IR wavelength region have been demonstrated in the last few decades,

by using silver halide crystalline fibers [5,6], hollow core fibers [7,8] and chalcogenide fibers [9–13]. Rave et al. [5] developed fiber bundles made of 100-9000 AgClBr fibers by multiple extrusion process. The fiber bundle areas and lengths were ranging from 5 to 20 mm^2 and from 5 to 60 cm, respectively. They obtained a cross-talk lower than 25% over a 5 cm long bundle. The fiber bundle loss ranged from 0.12 to 1.92 dB/cm at 10.6 μm in wavelength. Such high loss is likely to be attributed to the multiple extrusion process [5]. The same group later reduced the loss of these silver halide fibers down to 9.4 dB/m and 2.3 dB/m at 10.6 μm for bundles with 0.7 mm and 2.2 mm outer diameter, respectively [6]. Another potential solution is that of using hollow core fibers coated with Ag/AgI, as in the work by Gopal et al. [7], who have presented fiber bundles with up to 900 individual fibers. The bundle was however rigid due to the large required size of each hollow core, and only 2.5 cm in length; it had a loss of 9.7 dB/m at 10.6 µm in wavelength [7]. A longer bundle, 90 cm long, made of 245 hollow core borosilicate fibers has been also recently developed by Kobayashi et al. [8]. It exhibited a high transmission loss of the order of 14 dB/m between 3 and 4 μm in wavelength. They performed thermal imaging of objects at a temperature of 32 °C through a 30 cm long bundle [8]. Arguably, the closest technology yet reported that would be able to realize flexible low loss bundles is that employing chalcogenide glasses. Saito et al. [9] fabricated a fiber bundle consisting of 200 AsS core and FEP cladding fibers. This fiber bundle had a 2.2 mm outer diameter. Although this excellent work presented losses as low as 0.6 dB/m at 3.3 and 4.8 μm it offered a limited spatial resolution. Nishii et al. [10] have developed a fiber bundle made of 8400 AsS core and Teflon cladding fibers which was transparent between 1 and 7 μm. The cross section of this fiber bundle was rectangular (5.3 × 7.8 mm) and only the fiber ends were cemented together to make the bundle flexible. This fiber bundle was efficient for temperatures as low as 25 °C [10]. More recently, a fiber bundle with high spatial resolution made of 810000 As$_2$S$_3$ glass core and polyetherimide (PEI) polymer cladding with a cross section of 110 mm^2 has been developed by Zhang et al. [11]. The inter-core cross-talk was around 2.5% over a 5 cm long fiber bundle. In order to give mechanical flexibility to an otherwise fairly rigid bundle, they dissolved the PEI polymer in a solvent, which however resulted in increased cross-talk between adjacent fibers [11]. A fiber bundle of 2.2 × 2.2 mm of dimensions, made of 4000 As$_2$S$_3$ fibers was also realized by Chenard et al. [12]. The bundle transmits between 1.5 and 6.5 μm in wavelength. Although the bundle had a low numerical aperture (NA) of 0.3, they reduced the inter-core cross-talk thanks to a buffer layer of Polyethersulfone polymer around each fiber. Their attempt presents some dislocations due to the fabrication process [12]. More recently, Qi et al. [13] have fabricated a fiber bundle made of 200000 GeAsTeSe glass core and polyetherimide (PEI) polymer cladding [13]. Although they obtained a high number of pixels, the high transmission loss of 60 dB/m at 10 μm wavelength only allowed them to perform a thermal image of a human hand through a 5 cm long bundle [13]. Over that length, the inter-pixel cross-talk was around 1%. In conclusion, while multiple approaches have been proposed, achieving simultaneously good performance in terms of length, loss, mechanical flexibility, coherence and inter-core cross-talk is generally a fairly challenging task.

In this work, we focus on the development of a coherent fiber bundle which is compact, mechanically flexible and that allows thermal imaging of objects at temperatures down to those of a human body. We initially optimize the bundle to transmit radiation between 3 and 5.5 μm wavelengths. This is compatible with commercial thermal cameras based on cooled InSb detectors, which have the highest sensitivity in this spectral range [14]. To image even colder bodies we however wanted to choose a glass able to transmit at even longer wavelengths, to allow us to optimize the bundle for future operation with cheaper microbolometric cameras operating in the 8-14 μm spectral range. We have carefully designed our bundle and chosen its materials targeting a broad transmission band in the Mid-IR, good mechanical flexibility, and a high index contrast between core pixels and the cladding to minimize the inter-core cross-talk. The fabricated fiber bundle is mechanically

flexible and shows good imaging capabilities and low cross-talk. Thermal images of a human hand through a fiber bundle 1.1 mm thick and 62.5 cm long are demonstrated, which we believe represents a step forward towards the realization of practical Mid-IR thermal imaging bundles.

2. Material choice and characterization

The choice of core and cladding materials plays an important role in the development of a bundle that is mechanically flexible and possesses good thermal imaging properties. The core material must be transparent in the Mid-IR region, while for the cladding low Young's modulus materials like polymers allows improved robustness and flexibility as compared to an all-glass structure. For the core material, we selected the commercially available Vitron IG3 chalcogenide glass [15] because of its optical transmission between 3 and 12 μm and its high refractive index of 2.81 at λ = 3 μm [Fig. 1(a)]. The glass is made of $Ge_{30}As_{13}Se_{32}Te_{25}$ and its transition temperature and softening point are 275 °C and 360 °C, respectively [15]. To measure its loss, we fabricated an unclad fiber with a diameter of 240 μm, on which we performed a cutback measurement using a Fourier Transform Infrared (FTIR) spectrometer.
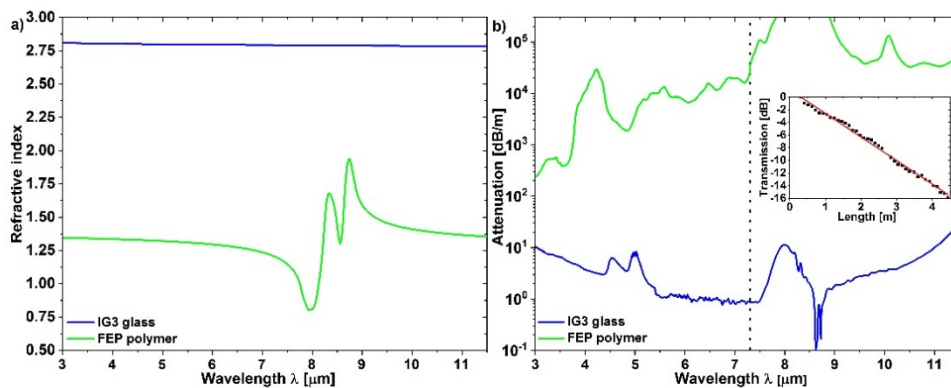

Fig. 1. (a) Refractive index of Vitron IG3 chalcogenide glass provided by Vitron [15] (blue curve) and of the FEP polymer (green curve) measured by the J.A. Woollam Co IR-VASE spectroscopic ellipsometer. (b) The blue curve represents Vitron IG3 glass loss measured on an uncladded fiber of 240 μm of diameter for λ between 3 and 5.4 μm combined with the loss measured on a fiber of 700 μm for λ between 5.4 and 11.5 μm. The inset shows the fiber transmission in dB at 4 μm in wavelength measured at different fiber lengths. The green curve represents the FEP polymer loss measured on a sample 0.86 mm thick for λ between 3 and 7.3 μm and on a sample 0.05 mm thick for λ between 7.3 and 11.5 μm. The dotted vertical line represents the delimitation between the FEP loss measurement on the 0.86 and 0.05 mm thick samples.

As a source, we used a Thorlabs SLS202L Stabilized Tungsten lamp, and the fiber transmission within 2.6-5.4 μm was measured with an ARCoptix FT-IR rocket spectrometer. 39 transmission spectra were measured by cutting the fiber every 10 cm. To extend the glass loss measurement to longer wavelengths (5.4-12 μm) we also performed another cutback measurement using a more conventional Varian 670 FTIR spectrometer. To confirm that the loss measurement was not a function of the fiber diameter, we used a different fiber, made of the same IG3 glass core, but with a FEP polymer cladding. The core diameter was even larger (700 μm), to minimize the fraction of modal power in the polymer cladding. The glass loss measurements of the two different fiber samples were comparable at 5.4 μm. Figure 1(b) shows the combined measured glass attenuation curve, while the inset shows the cutback measurement at 4 μm wavelength and its linear fit with a coefficient of determination R^2 of 0.9939. In the 3-5 μm wavelength range the IG3 loss is between 3 and 10.4 dB/m. Between 5.5 and 7.5 μm the IG3 glass has loss between 0.84 and 1.25 dB/m. At longer wavelengths, in the 8.75-10.5 μm wavelength range the glass loss is between 0.75 and 5 dB/m. Beyond 11 μm

the IG3 loss increases due to the glass multiphonon edge. The absorption peaks at 4.52 µm and at 7.8 µm are attributed to the Se-H bond, while the peak at 4.95 µm is due to the Ge-H bond [16]. Although the background loss of this commercial glass is already fairly high even before we structure it into a fiber bundle, we considered this to be adequate for this initial demonstration, knowing that it can be reduced by suitable distillation processes (i.e. vacuum distillation) in future works.

As a cladding material, we wanted a fluoropolymer with thermally compatible characteristics that would allow us to co-draw the two materials with a rod-in-tube technique. To select the most suitable cladding material, we performed two drawing tests using an IG3 glass rod and both a perfluoroalkoxy (PFA) and a Fluorinated Ethylene Propylene (FEP) polymer tube. The IG3-FEP combination was found to give the most stable fiber draw, with the least amount of diameter fluctuations. For this reason, we chose the FEP polymer as a cladding material. It is a known thermoplastic material with a low Young's modulus (~600 MPa) [17], and with melting point and processing temperatures of 260 and 370 °C, respectively [18]. Figure 1(a) shows the FEP polymer refractive index measured by using variable angle spectroscopic ellipsometer IR-VASE, J. A. Woollam Co., which covers the spectral range 840 - 5500 cm^{-1}. Spectra for angle of incidence of 45°, 50°, 55° and 60° were recorded (measuring 25 scans, 15 spectra per revolution, with wavenumber steps 8 cm^{-1}). At 3 µm wavelengths its refractive index was measured to be 1.345. The FEP polymer shows a refractive index change between 8 and 8.75 µm due to a large absorption peak.

To better support our modelling simulations shown in later sections, we also measured the attenuation of the cladding material. We used a Varian 670 FTIR spectrometer on a 0.86 ± 0.03 mm thick sample. Since the spectrometer was not capable of measuring the transmission of the FEP sample beyond 7.3 µm due to high material losses, the loss in the 7.3-12 µm wavelength range was measured on a thinner 0.05 mm sample. The attenuation of the FEP polymer is shown in Fig. 1(b). In the 3-5 µm wavelength range the polymer loss is between 241 dB/m and 29578 dB/m. Between 6 and 7 µm the polymer loss is between 6644 and 20387 dB/m. In proximity of the large absorption peak, the polymer loss is extremely high. Hence, we were unable to measure the FEP transmission spectrum between 7.96 and 8.75 µm. In the 9-11.5 µm wavelength range the FEP loss is between 33022 and 162888 dB/m. The absorption peaks at 4.23 and 5.57 µm are attributed to the -CF$_2$- bond and -CF = CF$_2$ double bond, respectively. The stretching vibration of the C-F lead to absorption in the 7.1-10 µm wavelength range [19]. Despite the extremely high loss of FEP, simulation results indicated that thanks to the high index contrast with the glass and the resulting large fraction of modal power into the core for the first few modes (greater than 99.8%), the total bundle loss would still be dominated by the IG3 bulk loss. Therefore we proceeded to fabricate the bundle.

3. Fiber bundle fabrication

To fabricate the bundle, we used a stack and draw technique. This method allows one to obtain a bundle in a single draw step and automatically maintain its coherence (i.e. end-to-end pixel spatial matching) during fabrication. Unlike in the layer winding method [20], where handling small fibers is challenging, with stack and draw method we can fabricate a fiber bundle with arbitrary pixel size, the dimension of which can be decided directly during the draw. To minimize the number of thermal processes and reduce the possibility of glass crystallization, we fabricated the bundle with a single stack and draw. We first fabricated a rod-in-tube preform made by an IG3 glass rod of 12 mm in diameter and an FEP polymer tube of 12 and 14 mm of inner and outer diameter, respectively. This was drawn into 170 m of fiber with 300 ± 8 µm outer diameter. The fiber was cut in 1200 12 cm long pieces which were stacked in a triangular lattice inside a PMMA holder with an inner hexagonal hole. The stack was then consolidated in a furnace and inserted in a FEP polymer tube of 12 and 14 mm of inner and outer diameter. The final preform was drawn into the desired bundle. From the

same preform, we drew bundles with two different sizes: a bundle with an outer diameter of 1.1 mm and core diameters of 22 µm, and another bundle with an outer diameter of 0.675 mm and core diameters of 13 µm. Both ends of each fiber bundle were then polished. A dedicated mold was designed to embed several bundles in a polymer and acrylic matrix so that they could be polished simultaneously. A cylinder of PMMA with multiple holes was realised. The fiber bundles were bent and both their ends were inserted into the holes of the PMMA cylinder and held in a place by a stainless steel holder. In this way both bundle ends were polished at the same time showing the same polishing quality. A VLST acrylic (Kemet) was poured into the bundle assembly to mold them together. Then, the whole assembly was polished using a water/Al_2O_3 powder solution.

The first step consisted on the lapping in a cast iron plate using different solutions with powder grain size of 9, 3, 1 and 0.25 µm. The second step was the polishing on a soft cloth plates using a 0.25 µm grain size solution. Following the polishing process, the PMMA and acrylic matrix were dissolved in an acetone bath. Micrographs of the polished fiber bundles of both sizes are shown in Fig. 2(a) and Fig. 2(b). As can be seen, the overall structure is maintained extremely well (with only a few pixels out of position), indicating the co-drawing process is well controlled. Figure 3 shows that despite its outer diameter of 1.1 mm, even the larger of the two bundles is mechanically flexible, which would certainly not have been possible if we had chosen a second glass as the cladding.
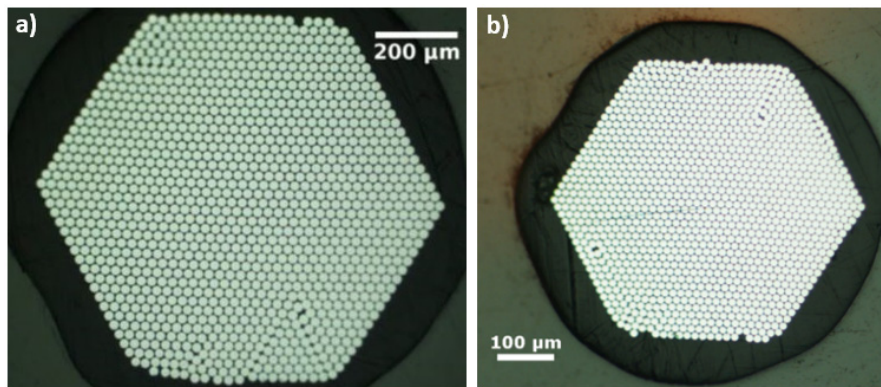

Fig. 2. Micrographs of Vitron IG3 glass core and FEP polymer cladding fiber bundle with outer and core diameter of (a) 1.1 mm and 22 µm and (b) 0.675 mm and 13 µm.
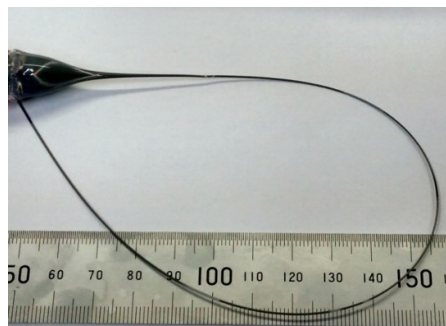

Fig. 3. Flexibility of the larger fiber bundle with an outer diameter of 1.1 mm.

4. Loss measurement

To assess the bundle imaging performance, it is essential to characterize its loss in the spectral range of interest for this work, i.e. between 3.6 and 4.9 µm where the InSb thermal camera available to us operates (see next Section). Measuring a fiber bundle loss is a cumbersome

procedure that has not been often undertaken in similar studies. Here we carried out the loss measurement by using the Arcoptix FTIR spectrometer with the same setup and method used to measure the IG3 core glass loss. After a first transmission measurement, the fiber bundle was shortened by 20 cm, its end was polished again and its transmission was re-measured. By repeating this operation 4 times, we obtained the fiber bundle transmission loss. In particular, we measured the attenuation of 2 different fiber bundles with 13 µm core diameter and of 2 different fiber bundles with 22 µm core diameter. By measuring the loss of 2 different bundles with the same core diameter it was possible to look at the reproducibility of the attenuation measurement. A difference of ± 1 dB/m between the 2 fiber bundles with equal core diameter was observed, which we attribute to residual scattering from imperfectly polished ends and to the coupling efficiency between the input of the fiber bundle and the Mid-IR lamp and between the output of the fiber bundle and the FTIR spectrometer. By averaging the attenuation of these two measurements, we obtained the loss curves shown in Fig. 4 (dashed and dashed-dotted lines). The attenuation of the 22 µm core diameter bundle is between 8 and 12 dB/m in the wavelength range from 3 to 4.5 µm. For the same wavelength range, the attenuation of the fiber bundle of 13 µm core diameter is between 7.5 and 17 dB/m. Both bundles present two absorption peaks at 3.53 and 4.52 µm both due to the Se-H bonds. The absorption peak at 4.95 µm is due to the Ge-H bonds of the IG3 glass [16]. The curves also show an additional peak at 4.23 µm, which is not visible in the glass loss curve shown in green. This is due to the -CF$_2$- bond in the polymer [19] [see Fig. 1(b)]. Due to light absorption in the very lossy FEP polymer cladding, the loss of both bundles is higher than that of the bulk glass. Since reducing the core diameter and increasing the wavelength increases the fraction of power guided in the lossy cladding, this peak is more accentuated in the smaller fiber bundle with 13 µm core diameter. For both bundles the loss differential with the bulk glass increases with wavelength. The losses of the 13 µm fiber bundle are lower than that of the 22 µm bundle at some wavelengths (between 3 and 3.6 µm, and also between 4.5 and 5.2 µm), possibly due to the measurements errors we have mentioned above.
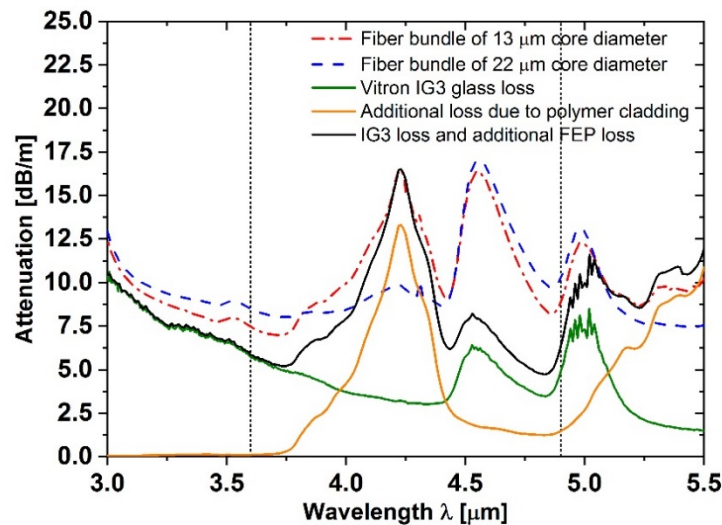

Fig. 4. Average attenuation of fiber bundles of 22 µm (dashed curve) and 13 µm (dashed-dotted curve) of core diameter and attenuation of the Vitron IG3 chalcogenide glass (green curve). The orange curve represents the additional loss due to the polymer cladding. The black curve represents the expected fiber bundle loss.

Since the fiber bundle is heavily multimoded, it is difficult to estimate theoretically its loss from first principles. For this reason we have used the method explained in the Appendix to combine a theoretical/numerical model with some experimentally inferred quantities. This

method allows to understand more about the origin of the various loss contributions. Moreover, this theoretical estimation gives us the possibility to predict the fiber bundle loss for long wavelength operation. Here we focus on the fiber bundle of 13 µm, for simplicity. In short, first we estimated the fraction of power in the cladding seen by an average ensemble of modes excited in the experiment, using the method explained in the Appendix. From this, we calculated the expected additional loss due to the FEP polymer, shown by the orange curve in Fig. 4. By adding this amount to the glass bulk loss (green curve), we obtained the expected fiber bundle loss shown by the black curve. The measured and calculated loss are identical at the polymer loss peak of 4.23 µm, where we fitted our data, but also agree well in the 5-5.5 µm range. The difference between measured and calculated loss in the 3-4 µm spectral range is attributed to some scattering at the core/clad interface. At 4.52 µm, in correspondence with the Se-H bond absorption, we see the maximum discrepancy, which likely indicates that additional Se-H bonds have been formed during fiber drawing. While these overall values of loss are still fairly high (generally better than some other reported works [7,8] but worse than others [9]), they are still low enough for the delivery of thermal images through a meter long fiber bundles.

5. Thermal imaging

Next, we performed a qualitative assessment of the thermal imaging properties of the polished fiber bundles, using a Xenics Onca MWIR 320 thermal camera consisting of a cooled Indium Antimonide (InSb) detector (1-5.5 µm). The thermal camera operates between 3.6 and 4.9 µm due to the presence of a spectral filter, identified by the vertical lines in Fig. 4. A 20×20 mm ceramic heating element shown in Fig. 5 was used as an infrared radiation source. Two chalcogenide lenses with antireflection coating for the wavelength range between 3.5 and 5 µm, were used. The first lens, with a numerical aperture and focal length of 0.86 and 1.873 mm, respectively, was used to focus the ceramic heating element onto the input surface of the fiber bundle. The second lens with a numerical aperture and focal length of 0.56 and 4 mm, respectively, was used to focus the image from the output surface of the fiber bundle onto the detector of the thermal camera. Figure 5 shows the experimental setup.
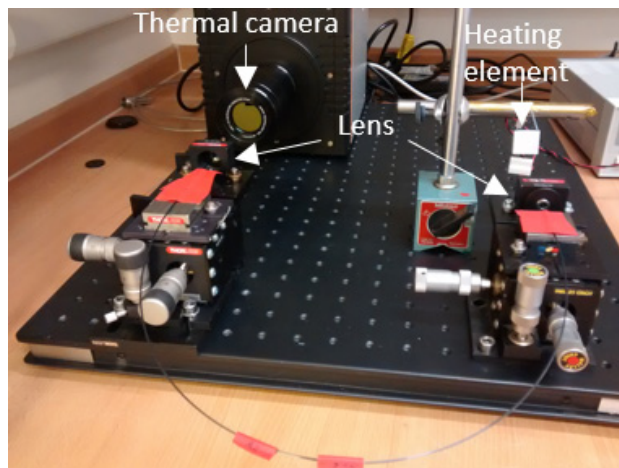

Fig. 5. Experimental setup for thermal imaging.

The temperature of the heating element was calibrated using a resistive temperature sensor placed onto its surface. Thermal images of the ceramic heating element at temperatures equal to 115 and 80 °C were transmitted through 1.15 m of the largest bundle (1.1 mm outer diameter) to the thermal camera. The bundle was arranged to form a 'u' shape, with a radius of curvature of ~15 cm, to test its performance in the presence of bending. These images are shown in Figs. 6(a) and 6(b), respectively, showing that the contours of the ceramic heating

element at 115 °C are sharp and well defined. It is clear that all pixels apart from few scattered ones transmit the same amount of light and therefore appear at a very similar temperature. On the bottom right of Fig. 6(a) a sequence of thermal images are displayed of the heating element at 115 °C, produced by changing the position of the input of the fiber bundle through the translation stage. Again, sharp edges can be seen. At lower temperatures, thermal imaging becomes more problematic because due to the fiber bundle loss an insufficient amount of radiation hits the detector. In fact, for a heating element at $T = 80$ °C, the image is less sharp.
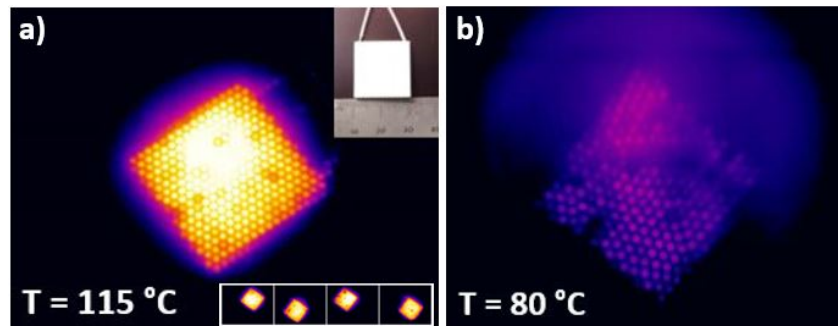

Fig. 6. Thermal image of a ceramic heating element at temperature (a) $T = 115$ °C and (b) $T = 80$ °C, through a fiber bundle 1.15 m long (1.1 mm outer diameter) performed by using the Xenics Onca MWIR 320 thermal camera. The insets of (a) show a sequence of thermal images of the heating element, produced by changing the position of the input of the fiber bundle through the translation stage.

To prove that lower temperature objects can still be imaged if one reduces the bundle length, we shortened the bundle to 62.5 cm and recorded thermal images of a human hand, as shown in Fig. 7. As can be seen, the hand is clearly visible and all the fingers clearly distinguishable. Also in this case, the pixels are almost at the same temperature. The insets show a sequence of thermal images performed by moving the hand. The thermal images on Figs. 6 and 7 have been both acquired using an integration time of 1.2 ms. Since colder objects as the human body are at a temperature closer to the room temperature, the thermal image appear noisier. To obtain a sharper image of the hand we applied a background subtraction. Figures 6 and 7 provide a proof of the full coherence of the fabricated bundle.
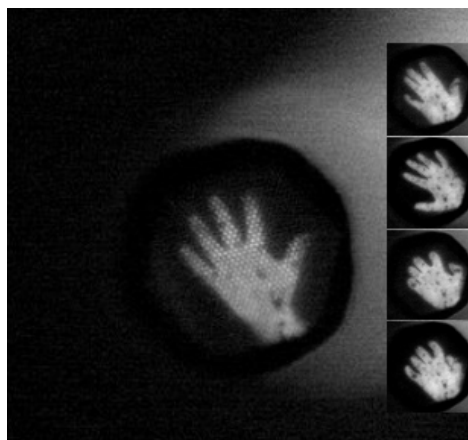

Fig. 7. Thermal image of a human hand through a fiber bundle 62.5 cm long (1.1 mm outer diameter) performed by using the Xenics Onca MWIR 320 thermal camera. The insets show a sequence of thermal images by moving the hand.

The sharp contours in the images above already indicate that over these lengths the inter-pixel cross-talk in the bundle is low. A further qualitative experiment was performed using a metal plate with inscribed letters. This was placed between the input of the 62.5 cm long fiber bundle and the ceramic heating element at 115 °C, to evaluate the presence and effect of cross-talk. Figure 8 shows that the image propagating through the bundle and reaching the thermal camera has sharp contours, with no evident inter-core cross-talk. We attribute this excellent performance to our initial choice of a high index contrast between the Vitron IG3 glass core and the FEP polymer cladding, which helps confining the power inside each pixel. Some beneficial contribution might also be played by the high cladding loss, which severely attenuates the highest order modes in each pixel that would otherwise be the main source of cross-talk. Such an imaging performance would not be possible with fiber bundles with lower numerical aperture fabricated, for example, using silver halide crystalline fibers or all glass AsS core-AsS cladding fibers.
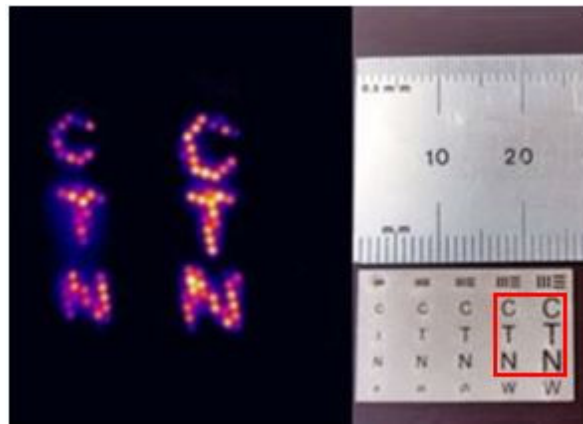

Fig. 8. Thermal image through a fiber bundle 62.5 cm long (1.1 mm outer diameter) by placing a metal target with inscribed letters between the input of the fiber bundle and the ceramic heating element at temperature $T = 115$ °C.

In order to estimate the cross-talk more quantitatively, a single pixel of the 62.5 cm long fiber bundle was excited using a Mid-IR incandescent lamp. An iris was used to block the infrared radiation outside a small spot and prevent it from reaching pixels other than a randomly selected one in isolation, or the same pixel with its 6 surrounding neighbors (inset of Fig. 9).

From the images we extracted cross-sectional intensity profiles along selected direction, as shown in Fig. 9. The green curve and the blue curve represent the intensity profile when a single pixel and when 7 pixels are excited, respectively.

From this graph it is clear that when the light is focused in a single pixel the level of cross-talk into the adjacent cores is extremely low. We used the 7 pixel trace to identify the position of the neighboring pixels (1st and 2nd pixels), which was then used to calculate the cross-talk. The cross-talk was calculated on the single pixel excitation curve (green) as the ratio between the integrated cross-sectional intensity of one surrounding core to the integrated cross-sectional intensity for the excited core. In order to obtain a more reliable measurement, we averaged the cross-talks obtained for the 1st and the 2nd pixel. Since the cross-talk measurement was performed on a 62.5 cm long bundle, we scaled the cross-talk measurement for a meter long bundle considering that the inter-core cross-talk increases proportionally with the bundle length due to the high numerical aperture. The measured cross-talk was estimated to be around −13.7 dB/m.
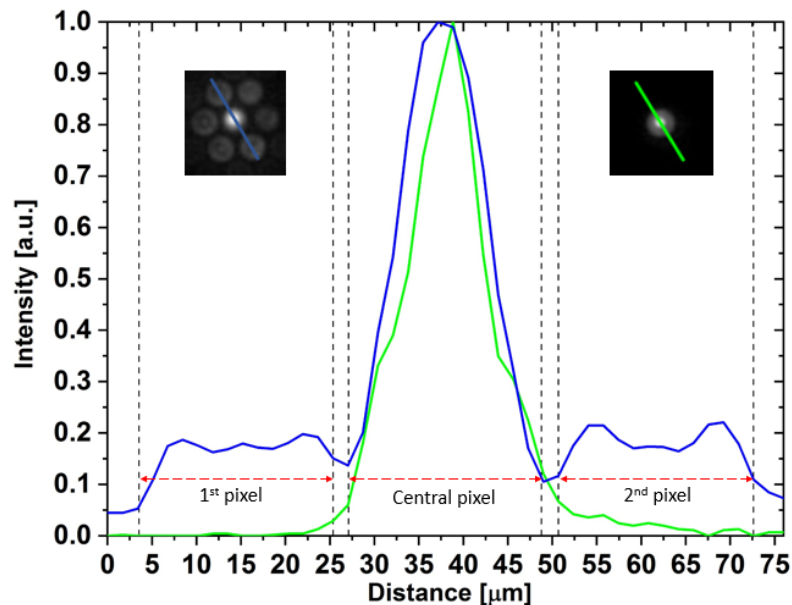
Fig. 9. Intensity distribution at the output of the fiber bundle 62.5 cm long (1.1 mm outer diameter) by exciting several cores (blue curve) and a single core (green curve). Inset shows perpendicular cut of single pixel excited fiber (right upper corner – green) and excitation of single pixel with 6 nearest neighbors (left upper corner – blue).

6. Bundle design consideration for 9-12 um wavelength operation

Having fabricated a bundle for operation with a 3-5 μm cooled-sensor camera, we have then conducted a modelling exercise to understand how such a bundle would need to scale to operate in the 9-12 μm region, where less expensive microbolometric thermal cameras operate. Since the calculation of the expected loss for the fiber bundle of 13 μm was in fairly good agreement with the experimental measurement, we have used the same method to estimate the loss of bundles with the same materials and pixel diameter to pixel distance ratio, but a larger core diameters (22, 40, 80 and 100 μm). For all these cases, the dashed curves of Fig. 10 represent the simulated attenuation of the fundamental mode only, while the solid curves represent the estimated attenuation of an ensemble of several modes. In both cases we have used the procedure reported in the Appendix. As can be seen, the difference between the two approaches decreases with core diameter increasing and becomes almost negligible close to 11 μm for core diameters of 80 and 100 μm. A grey hashed bar was placed in the spectral region where the FEP polymer loss were too high to be measured (7.96 - 8.75 μm wavelength).

In the region between 9 and 11 μm, the fiber bundles with 13 and 22 μm pixel diameter have impractically high losses approaching 100 dB/m, indicating that in order to scale with the wavelength, the core diameter should be larger. A fiber bundle of 40 μm has losses between 10.7 and 35.5 dB/m from 9 to 11 μm, showing its minimum at 9.64 μm. In the same wavelength range, bundles with 80 μm and 100 μm would have more reasonable losses of 3.6 to 11.5 dB/m and 2.9 to 10.7 dB/m, respectively. This is not so much higher than the bulk loss of the glass (shown in brown in Fig. 10), despite the extremely high loss of the FEP polymer at these wavelengths. From this, we conclude that in order to achieve a reasonable loss for thermal imaging in the long wavelength IR region, bundles with pixel sizes of the order of 80 μm or above should be used. Using such large pixels would have the obvious disadvantage of increasing the overall diameter of the bundle, which might compromise its flexibility. One workaround could be that of letting individual fibers or subsets of the total bundle

independent and only attaching them at the bundle extremities to form a coherent imaging system.
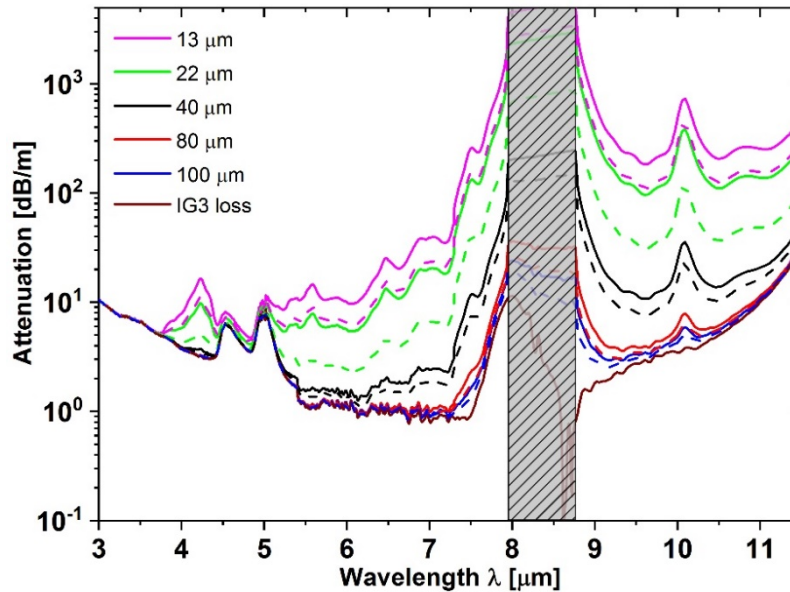

Fig. 10. Attenuation calculated by using the procedure explained in the Appendix for core diameter of 13 (solid magenta curve), 22 (solid green curve), 40 (solid black curve), 80 (solid red curve) and 100 μm (solid blue curve). The dashed curves represent the attenuation simulated of the fundamental mode. The brown curve represents the IG3 loss. The grey hashed bar represents the spectral region where the FEP polymer loss were too high to be measured.

7. Conclusions

We have fabricated two flexible coherent Mid-IR fiber bundles made of 1200 chalcogenide core and fluoro-polymer cladding fibers using the stack and draw method. The fiber bundles had an outer diameter of 1.1 mm and 0.675 mm, resulting in pixel sizes of 22 and 13 μm, respectively. Using the larger bundle, sharp edged thermal images of objects at temperatures down to 80 °C were obtained through a bent bundle 1.15 m long. A thermal image of a human hand was also performed through a shorter bundle 62.5 cm long. An inter-pixel cross-talk as low as −13.7 dB/m was measured, which was sufficient to avoid degradation of the thermal imaging quality, and stemmed from the high index contrast between the glass core and polymer cladding. This result can be improved further in future works by increasing the lengths over which thermal imaging of room temperature objects can be performed. To do so, one would need to decrease the fiber bundle loss, by either changing or purifying the core material, or by further enlarging the pixel size to reduce the interaction of the modes with the lossy polymer cladding. To capture endoscopic thermal images using lower cost and simpler long wavelength IR microbolometric thermal cameras, our modelling study indicates that considerably larger pixel dimensions, of the order of 80 μm, would be needed in order to minimize the fraction of modal power in cladding.

8. Appendix

Here we highlight a procedure to estimate the overlap of a single mode or an ensemble of modes with the cladding of each individual pixel, which can then be used to predict how the performance of this family of bundles scales with wavelength and pixel size. As an illustrative example we use the 13 μm pixel fiber bundle discussed above. We start by

determining from experimental measurements the fraction of power in the cladding (ηClad) that would be responsible for the measured loss. To do so, we subtract the loss of the bulk glass from the measured loss of the bundle, to obtain the additional loss caused by the bundle fabrication. By dividing this amount by the FEP polymer loss across the wavelength range, we obtain ηClad. This is shown in Fig. 11 (green curve). Here we can see three components: a) one that decreases with wavelength at 3 to 4 µm, which we attribute to additional scattering at the core/clad interface. This becomes negligible at longer wavelengths; b) two peaks at 3.53 and 4.52 µm that are due to chemical interactions between the glass and the polymer that cause additional absorption peaks; and c) a wavelength increasing contribution that is due to an increased power overlap of the optical mode with the lossy polymer at longer wavelengths. Multiplying this overlap by the known loss of the polymer produces the additional loss due to the polymer. In order to extrapolate this latter contribution to wavelengths outside the measurement range of our instrument, we used the following procedure. For large V-number fibers like those in this work, an asymptotic analytical expression exists for ηClad [21]:

$$\eta_{clad} \approx \frac{U^2}{V^3} \qquad (1)$$

where U and V are the standard normalized effective index and frequency of fiber optics, respectively. From this, the dependence of the cladding overlap on the wavelength λ can be expressed as:

$$\eta_{clad} = k_1 \lambda^3 e^{-k_2 \cdot \lambda} \qquad (2)$$

where k_1 is a constant which depends on the excited modes and $k_2 = 2/(2\pi\rho NA)$ only depends on the fiber's known structural parameters such as the core radius ρ and the numerical aperture NA [21]. The validity of Eq. (2) was verified through modelling, as follows. Since the fiber bundle can be seen as an array of optical fibers with low/negligible cross-talk between them (as shown above), we modeled a single fiber made of IG3 glass core and FEP cladding using Finite Element Method (FEM) simulations in Comsol Multiphysics. The complex refractive index of the glass and of the polymer shown in Fig. 1 were used, and a Perfectly Matched Layer (PML) was employed to avoid reflections from the outer boundaries [22]. The core diameter was set to 13 µm. The fraction of power in the cladding of the fundamental mode (ηClad$_{FM}$) was simulated at wavelengths between 3 and 10 µm. For the fundamental mode, this equation was found to agree fairly well with the simulated ηClad$_{FM}$, with small differences likely arising from the approximate nature of (1). We further observed that if we used k_1 as free parameter in the fit of the simulation values with the Eq. (2) in the 3-12 µm spectral range, the agreement between formula and simulations improved. The simulated ηClad$_{FM}$ (black squares) and its fit with Eq. (2) are shown in Fig. 11 between 3 and 5.5 µm (blue curve). Since these fiber bundles are heavily multimoded, in practice the IR radiation from the object to be imaged excites a combination of modes. The average ensemble of the excited modes has a larger overlap with the polymer than just the fundamental mode. From the value of the experimentally extracted fractional power in the polymer (green curve) at 4.23 µm, the position of the main polymer peak observed in Fig. 4, we calculated the value of the constant k_1, by using Eq. (2). The calculated constant k_1 takes into account of the average ensemble of the excited modes of our bundle. We then estimated the spectral behavior of the fraction of power in the cladding for a fiber with a core of 13 µm, and this is shown in Fig. 11 (dashed red curve). Next, we applied the same method to a fiber with a core diameter of 22 µm, for which we also had experimental results (see Fig. 4). As one would expect, enlarging the core causes a lower cladding overlap due to the ensemble of modes, which explains why the larger bundle was found to have overall lower loss. Since this semi-empirical method showed a good agreement between the measurements and the simulations for cores of 13 and 22 µm, we then also used it to predict the behavior of bundles with larger

pixel dimensions. The cladding overlap due to the average ensemble of the excited modes cannot be calculated accurately for the larger core sizes as it depends on the number of guided and excited modes, on the individual modal excitation at launch, on the intermodal mode coupling and external perturbation, etc. Nonetheless, from Eq. (1) we can derive the dependence of the overall fraction of power in the cladding due to the excitation of several modes as a function of the core diameter r:

$$\sum \eta_{clad} = \frac{k_3 e^{-\frac{k_4}{r}}}{r^3}$$

(3)

where r is the core radius, k_3 is a constant which depends on the excited modes and $k_4 = 2\lambda/(2\pi NA)$ [21].
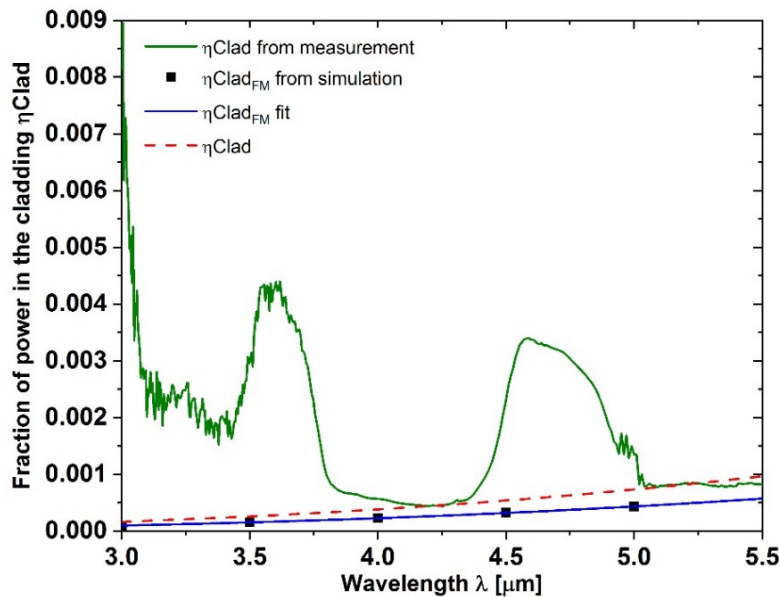

Fig. 11. Fraction of power in the cladding of the bundle of 13 µm calculated from measurement (green curve). Fraction of power in the cladding of the fundamental mode simulated on a fiber with core of 13 µm (black squares) and its fit (blue curve). Estimated fraction of power in the cladding (dashed red curve).

We then estimated the dependence of the overall fraction of power in the cladding with the core diameter, by fitting the cladding overlap extracted from measurements for cores of 13 and 22 µm, with Eq. (3). With this estimated overlap we could then produce the various curves in Fig. 10. Note that this is a big approximation, given that the number of excited modes might also change from bundle to bundle and that there was a non-negligible experimental error in the measurements, and it should be therefore only considered as a general guidance only. However, theory predicts that the overall fraction of power in the cladding should become decreasingly smaller with increasing pixel size. We therefore believe that the general conclusions shown in Fig. 10 are to first order approximation correct.

Funding

Acknowledgments

References

1. E. F. J. Ring and K. Ammer, "Infrared thermal imaging in medicine," Physiol. Meas. **33**(3), R33–R46 (2012).
2. B. F. Jones, "A Reappraisal of the Use of Infrared Thermal Image Analysis in Medicine," IEEE **17**(6), 1019–1027 (1998).
3. A. Glowacz and Z. Glowacz, "Diagnosis of three-phase induction motor using thermal imaging," Infrared Phys. Technol. **81**, 7–16 (2017).
4. H. H. Hopkins and N. S. Kapany, "A Flexible Fibrescope, using Static Scanning," Nature **173**(4392), 39–41 (1954).
5. E. Rave, L. Nagli, and A. Katzir, "Ordered bundles of infrared-transmitting AgClBr fibers: optical characterization of individual fibers," Opt. Lett. **25**(17), 1237–1239 (2000).
6. Y. Lavi, A. Millo, and A. Katzir, "Flexible ordered bundles of infrared transmitting silver-halide fibers: design, fabrication, and optical measurements," Appl. Opt. **45**(23), 5808–5814 (2006).
7. V. Gopal, J. A. Harrington, A. Goren, and I. Gannot, "Coherent hollow-core waveguide bundles for infrared imaging," Opt. Eng. **43**(5), 1195–1199 (2004).
8. T. Kobayashi, T. Katagiri, and Y. Matsuura, "Fabrication of bundle-structured tube-leaky optical fibers for infrared thermal imaging," Proc. SPIE, **10058**, 100580X (2017).
9. M. Saito, M. Takizawa, S. Sakuragi, and F. Tanei, "Infrared image guide with bundled As-S glass fibers," Appl. Opt. **24**(15), 2304–2309 (1985).
10. J. Nishii, T. Yamashita, T. Yamagishi, C. Tanaka, and H. Sone, "Coherent infrared fiber image bundle," Appl. Phys. Lett. **59**(21), 2639–2641 (1991).
11. B. Zhang, C. Zhai, S. Qi, W. Guo, Z. Yang, A. Yang, X. Gai, Y. Yu, R. Wang, D. Tang, G. Tao, and B. Luther-Davies, "High-resolution chalcogenide fiber bundles for infrared imaging," Opt. Lett. **40**(19), 4384–4387 (2015).
12. F. Chenard, O. Alvarez, D. Gibson, L. Brandon Shaw, and J. Sanghera, "Mid-Infrared Imaging Fiber Bundle," Proc. SPIE **10181**, 101810V (2017).
13. S. Qi, B. Zhang, C. Zhai, Y. Li, A. Yang, Y. Yu, D. Tang, Z. Yang, and B. Luther-Davies, "High-resolution chalcogenide fiber bundles for longwave infrared imaging," Opt. Express **25**(21), 26160–26165 (2017).
14. Hamamatsu, "Infrared Detectors," https://www.hamamatsu.com/resources/pdf/ssd/infrared_kird0001e.pdf.
15. Vitron, "Vitron IG3," http://www.vitron.de/datasheets/VITRON%20IG-3%20Datenblatt%20Juni%202014%20.pdf.
16. G. E. Snopatin, V. S. Shiryaev, V. G. Plotnichenko, E. M. Dianov, and M. F. Churbanov, "High-Purity Chalcogenide Glasses for Fiber Optics," Inorg. Mater. **45**(13), 1439–1460 (2009).
17. Du Pont, "FEP handbook," http://www.rjchase.com/fep_handbook.pdf.
18. Fluorotherm, "FEP Properties," https://www.fluorotherm.com/technical-information/materials-overview/fep-properties/.
19. A. M. S. Galante, O. L. Galante, and L. L. Campos, "Study on application of PTFE, FEP and PFA fluoropolymers on radiation dosimetry," Nucl. Instrum. Methods Phys. Res. A **619**(1-3), 177–180 (2010).
20. N. S. Kapany, *Fiber Optics*, (Academic Press, 1967).
21. A. W. Snyder, "Asymptotic Expressions for Eigenfunctions and Eigenvalues of a Dielectric or Optical Waveguide," IEEE Trans. MTT **17**(12), 1130–1138 (1969).
22. J. P. Berenger, "A Perfectly Matched Layer for the Absorption of the Electromagnetic Waves," J. Comput. Phys. **114**(2), 185–200 (1994).